Full Length Article

Free convection in a square cavity filled by a porous medium saturated by a nanofluid: Viscous dissipation and radiation effects

CrossMark

M. Ghalambaz [a,*], M. Sabour [a], I. Pop [b]

[a] Department of Mechanical Engineering, Dezful Branch, Islamic Azad University, Dezful, Iran
[b] Department of Applied Mathematics, Babeş-Bolyai University, 400084 Cluj-Napoca, Romania

ABSTRACT

The influence of the viscous dissipation and radiation effects on the natural convection heat transfer in a square cavity filled with porous media saturated with a nanofluid is studied. The vertical walls of the cavity are subject to finite temperature difference while the top and bottom walls of the cavity are insulated. The Buongiorno's nanofluid model, incorporating the Brownian motion and thermophoresis effects, is employed. The governing equations, in nondimensional form, are written in the weak form and solved using the finite element method. The influences of viscous dissipation and radiation effects on the concentration distribution of nanoparticles are discussed. The average and local Nusselt numbers are reported for various values of viscous dissipation (Eckert number) and radiation effects. The results show that the Nusselt numbers at the hot and cold walls are not equal due to the presence of viscous dissipation effects. The raise of Eckert number decreases the Nusselt number at hot wall, but it increases the Nusselt number at the cold wall. It is also found that the increase of Lewis number enhances the heat transfer in the cavity.

© 2016 Karabuk University. Publishing services by Elsevier B.V. This is an open access article under the CC BY-NC-ND license (http://creativecommons.org/licenses/by-nc-nd/4.0/).

1. Introduction

The heat transfer of nanofluids in porous media has gained considerable attention and many valuable studies have been performed in this subject. Consideration of the heat released by viscous dissipation depends on the other thermal sources, influencing the heat transfer in the fluid motion such as localized heat sources or sinks or buoyancy forces induced by heated or cooled walls. The heat released by viscous dissipation in natural convection could be significant in various devices, subject to large decelerations or which operate at high rotational speeds or stronger gravitational fields and in processes wherein the scale of the process is very large [1]. The flat plate solar collectors, supported with metallic porous foams indeed are cavities subject to internal heat generation due to solar radiation. The heat transfer in metal porous foams has found many industrial applications such as heat exchangers [2] and electronic components [3]. The radiation heat transfer of nanofluids has found applications in solar systems for direct absorption of solar radiation as discussed in Luo et al., Karami et al. and Menbari and Alemrajabi [4–6].

Different aspects of the convective heat transfer of nanofluids have been studied in many previous studies. For instance, Sun and Pop [7] have studied the free convective heat transfer of nanofluids in a porous triangle cavity. Ghalambaz et al. [8] have studied the effect of presence of nanoparticles on the convective heat transfer of nanofluids in a cavity filled with high conductive metal porous foams. Noghrehabadi et al. [9–11] have analyzed the free convective heat transfer of nanofluids in the boundary layer. Ghalambaz and Noghrehabadi [12], Ghalambaz et al. [13] as well as Zargartalebi et al. [14,15] have studied the effect of Brownian motion and thermophoresis forces on the boundary later natural convective heat transfer of nanofluids in porous media. Sheremet and Pop [16] have examined the conjugate heat transfer effects on the natural convective heat transfer of nanofluids. Sheremet et al. [17] have examined the effect of presence of nanoparticles and different thermal boundary conditions [18] on the natural convective heat transfer of nanofluids in a cavity filled with a porous medium.

The radiation effect and viscous dissipation are two important aspects of heat transfer in porous media, which were well studied in previous researches. Saeid and Pop [19] examined the effect of viscous dissipation on the natural convection heat transfer in a porous cavity. The authors [19] reported that the Nusselt number at hot wall is a decreasing function of the viscous dissipation parameter (Eckert number). Hussain and Pop [20] have studied the radiation effects over an inclined plate embedded in porous media. Mahdy and Chamkha [21] have examined the effect of viscous

* Corresponding author. Tel.: +98 61 42420601.
E-mail address: m.ghalambaz@iaud.ac.ir (M. Ghalambaz).
Peer review under responsibility of Karabuk University.

dissipation on the mixed convection in porous media. Considering the nanofluids in porous media, RamReddy et al. [22] and Chamkha et al. [23] have examined the effect of viscous dissipation on the boundary layer convective heat transfer of nanofluids. Rashad et al. [24] have studied the effect of viscous dissipation on the natural convective heat transfer of nanofluids assuming a homogeneous distribution of nanoparticles in the nanofluid and porous media.

Influences of skin friction coefficient, Brownian and thermophoresis forces on the third grade nanofluid are studied by Hussian et al. [25]. They have considered thermal radiation and MHD flow applicable in engineering issues such as heat exchangers and solar collectors. Shehzad et al. [26], have examined the effects of thermal radiation and internal heat generation in a nanofluid over a stretching surface. In another study, Shehzad et al. [27] have examined the effect of MHD (Magneto-hydro-Dynamic) flow on the Oldroyd-B nanofluid.

Recently, Makinde et al. [28] have investigated the MHD flow in a porous medium including the radiation effects. They examined the influence of viscous dissipation and magnetic field on the heat transfer over a vertical flat plate. The results show that boosting of magnetic field and Eckert number reduces heat transfer rate. Makinde [29] surveyed boundary layer flow about a flat plate in the presence of viscous dissipation effect for different types of nanofluids. Moreover, different types of water base nanofluids including Al_2O_3 and Cu in a porous medium have been examined over a flat plate by Motsumi and Makinde [30] and in a pipe by Khamis and Makinde [31]. The results indicate that the nanofluid containing Cu nanoparticles produces better heat transfer enhancement.

The review of the literature shows that the effect of viscous dissipation and radiation effects for nanofluids considering a non-homogenous model, incorporating the Brownian motion and thermophoresis forces, have not been addressed yet in a cavity. The present study aims to examine the influence of the viscous dissipation and radiation effects on the natural convective heat and mass transfer of nanofluids in a square cavity using the non-homogeneous model of nanofluids by employing the Buongiorno's mathematical model.

2. Basic equations

Consider the free convection flow of a nanofluid in a square cavity of size L filled with a nanofluid-saturated porous medium. There is a temperature difference between the isothermal vertical (right and left) walls while the horizontal walls (top and bottom) are well insulated. The cavity walls are assumed rigid and impermeable. The left vertical wall is assumed at the constant high temperature of T_h while the right vertical wall is at low temperature of T_c. A schematic representation of physical model, boundary conditions and the coordinate system is illustrated in Fig. 1.

It is assumed that the nanoparticles are well dispersed in the base fluid and the suspension is stable due to employed surface charges methods or presence of surfactants, which prevents nanoparticles from agglomeration and deposition on the porous matrix [32,33]. Further, the following assumptions are applied:

  (a) Porous medium is saturated with a nanofluid fluid
  (b) The fluid is assumed to be gray emitting and absorbing but non-scattering
  (c) The fluid and medium are in local thermal equilibrium everywhere inside the medium.

The Darcy–Boussinesq approximation is employed. Homogeneity and local thermal equilibrium in the porous medium are assumed. We consider a medium which its porosity is denoted by ε and permeability by K. The following are the four field equations for invoking
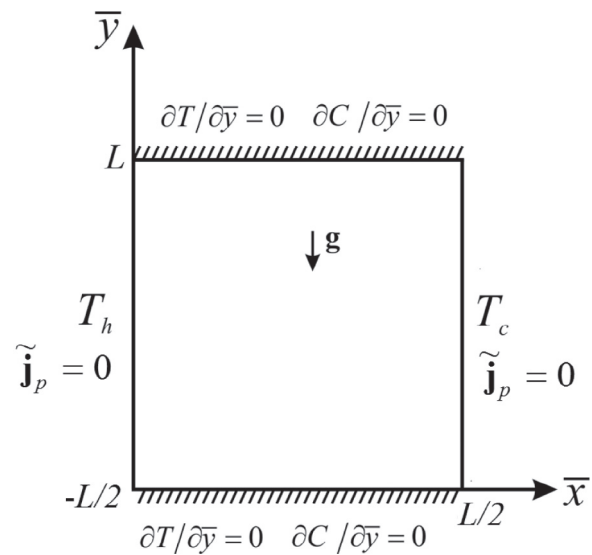

Fig. 1. Physical model and coordinate system.

the conservation of total mass, momentum, thermal energy, and nanoparticles, respectively (see [32–34])

$$\nabla \cdot V = 0, \tag{1}$$

$$0 = -\nabla P - \frac{\mu}{K}V + [C\rho_p + (1-C)\rho_{f0}(1-\beta(T-T_c))]g, \tag{2}$$

$$\sigma\frac{\partial T}{\partial t} + (V \cdot \nabla)T = \alpha_m\nabla^2 T + \delta\left(D_B\nabla C \cdot \nabla T + \frac{D_T}{T_c}\nabla T \cdot \nabla T\right) - \nabla \cdot q_r + \Phi, \tag{3}$$

$$\rho_p\left(\frac{\partial C}{\partial t} + \frac{1}{\varepsilon}(V \cdot \nabla)C\right) = -\nabla \cdot j_p, \tag{4}$$

where V is the Darcy velocity vector, T is the fluid temperature, C is the nanoparticle volume fraction, t is the time, p is the fluid pressure, $\mathbf{g}$ is the gravity vector, D_B is the Brownian diffusion coefficient, D_T is the thermophoretic diffusion coefficient, $j_p = -\rho_p\left[D_B\nabla C + \left(\frac{D_T}{T_c}\right)\nabla T\right]$ is the nanoparticles mass flux, ρ_{f0} is the reference density of the fluid. In the above equations, α_m, μ, ρ_p denote the effective thermal diffusivity of the porous medium, the dynamic viscosity, nanoparticle mass density, respectively. δ and σ are quantities defined by $\delta = \frac{\varepsilon(\rho c_p)_p}{(\rho c_p)_f}$ and $\sigma = \frac{(\rho c_p)_m}{(\rho c_p)_f}$. C_p is the heat capacity at constant pressure, $(\rho c_p)_f$ is heat capacity of the base fluid, $(\rho c_p)_p$ is effective heat capacity of the nanoparticle material, $(\rho c_p)_m$ is effective heat capacity of the porous medium, β is the coefficient of thermal expansion, q_r is the radiation flux and Φ is the viscous dissipation term.

The flow is assumed to be slow so that the advective term and the Forchheimer quadratic term do not appear in the momentum equation. In keeping with the Boussinesq approximation and an assumption that the nanoparticle concentration is dilute, and with a suitable choice for the reference pressure, we can linearize the momentum equation and write Eq. (2) as

$$0 = -\nabla P - \frac{\mu}{K}V + [C(\rho_p - \rho_{f0}) + \rho_{f0}(1-\beta(T-T_c)(1-C_0))]g. \tag{5}$$

We consider the Rosseland approximation for radiation [30]

$$q_r = -\frac{4\sigma_{SB}}{3a_R}\left(\frac{\partial T^4}{\partial \bar{x}} + \frac{\partial T^4}{\partial \bar{y}}\right) \tag{6}$$

where a_R is the Rosseland mean spectral absorption coefficient and σ_{BS} is the Stefan–Boltzmann constant. Expanding T^4 about T_∞ using Taylor series and neglecting higher order terms [35] results in

$$T^4 \approx 4TT_\infty^3 - 3T_\infty^4 \tag{7}$$

The basic equations for the problem under consideration can be written, in Cartesian coordinates $\bar{x}$ and $\bar{y}$, after the pressure p is eliminated from Eq. (5) by cross-differentiation, as

$$\frac{\partial u}{\partial \bar{x}} + \frac{\partial v}{\partial \bar{y}} = 0, \tag{8}$$

$$0 = -\frac{\mu}{K}\left(\frac{\partial u}{\partial \bar{y}} - \frac{\partial v}{\partial \bar{x}}\right) + g\left(\rho_p - \rho_{f0}\right)\frac{\partial C}{\partial \bar{x}} - (1-C_0)\rho_{f0}\beta g\frac{\partial T}{\partial \bar{x}}, \tag{9}$$

$$u\frac{\partial T}{\partial \bar{x}} + v\frac{\partial T}{\partial \bar{y}} = \alpha_m\left(\frac{\partial^2 T}{\partial \bar{x}^2} + \frac{\partial^2 T}{\partial \bar{y}^2}\right) + \delta\left\{D_B\left(\frac{\partial C}{\partial \bar{x}}\frac{\partial T}{\partial \bar{x}} + \frac{\partial C}{\partial \bar{y}}\frac{\partial T}{\partial \bar{y}}\right) \right.$$
$$\left. + \frac{D_T}{T_c}\left[\left(\frac{\partial T}{\partial \bar{x}}\right)^2 + \left(\frac{\partial T}{\partial \bar{y}}\right)^2\right]\right\} + \frac{16\sigma_{SB}T_\infty^3}{3a_R}\left(\frac{\partial^2 T}{\partial \bar{x}^2} + \frac{\partial^2 T}{\partial \bar{y}^2}\right) \tag{10}$$
$$+ \frac{\mu}{K(\rho c_p)_f}(u^2 + v^2),$$

$$\frac{1}{\varepsilon}\left(\frac{\partial C}{\partial \bar{x}} + \frac{\partial C}{\partial \bar{y}}\right) = D_B\left(\frac{\partial^2 C}{\partial \bar{x}^2} + \frac{\partial^2 C}{\partial \bar{y}^2}\right) + \left(\frac{D_T}{T_c}\right)\left(\frac{\partial^2 T}{\partial \bar{x}^2} + \frac{\partial^2 T}{\partial \bar{y}^2}\right) \tag{11}$$

where u and v are the velocity components along $\bar{x}$ and $\bar{y}$ directions, respectively. Introducing a stream function $\bar{\psi}$ defined by

$$u = \frac{\partial \bar{\psi}}{\partial \bar{y}}, \quad v = -\frac{\partial \bar{\psi}}{\partial \bar{x}} \tag{12}$$

ensures identical satisfaction of Eq. (8). We are then left with the following equations taking into account steady-state regime

$$\frac{\partial^2 \bar{\psi}}{\partial \bar{x}^2} + \frac{\partial^2 \bar{\psi}}{\partial \bar{y}^2} = -\frac{(1-C_0)\rho_{f0}gK\beta}{\mu}\frac{\partial T}{\partial \bar{x}} + \frac{\rho_p - \rho_{f0}}{\mu}gK\frac{\partial C}{\partial \bar{x}}, \tag{13}$$

$$\frac{\partial \bar{\psi}}{\partial \bar{y}}\frac{\partial T}{\partial \bar{x}} - \frac{\partial \bar{\psi}}{\partial \bar{x}}\frac{\partial T}{\partial \bar{y}} = \alpha_m\left(\frac{\partial^2 T}{\partial \bar{x}^2} + \frac{\partial^2 T}{\partial \bar{y}^2}\right) + \delta\left\{D_B\left(\frac{\partial C}{\partial \bar{x}}\frac{\partial T}{\partial \bar{x}} + \frac{\partial C}{\partial \bar{y}}\frac{\partial T}{\partial \bar{y}}\right) \right.$$
$$\left. + \frac{D_T}{T_c}\left[\left(\frac{\partial T}{\partial \bar{x}}\right)^2 + \left(\frac{\partial T}{\partial \bar{y}}\right)^2\right]\right\} + \frac{16\sigma_{SB}T_\infty^3}{3a_R}\left(\frac{\partial^2 T}{\partial \bar{x}^2} + \frac{\partial^2 T}{\partial \bar{y}^2}\right)$$
$$+ \frac{\mu}{K(\rho c_p)_f}\left(\left(\frac{\partial \bar{\psi}}{\partial \bar{x}}\right)^2 + \left(\frac{\partial \bar{\psi}}{\partial \bar{y}}\right)^2\right) \tag{14}$$

$$\frac{1}{\varepsilon}\left(\frac{\partial \bar{\psi}}{\partial \bar{y}}\frac{\partial C}{\partial \bar{x}} - \frac{\partial \bar{\psi}}{\partial \bar{x}}\frac{\partial C}{\partial \bar{y}}\right) = D_B\left(\frac{\partial^2 C}{\partial \bar{x}^2} + \frac{\partial^2 C}{\partial \bar{y}^2}\right) + \left(\frac{D_T}{T_c}\right)\left(\frac{\partial^2 T}{\partial \bar{x}^2} + \frac{\partial^2 T}{\partial \bar{y}^2}\right). \tag{15}$$

Introducing the following dimensionless variables

$$x = \bar{x}/L, \quad y = \bar{y}/L, \quad \psi = \bar{\psi}/\alpha_m, \quad \theta = \frac{T - T_c}{\Delta T}, \quad \varphi = C/C_0, \tag{16}$$

where $\Delta T = T_h - T_c$. Substituting Eq. (16) into Eqs. (13)–(15), we obtain

$$\frac{\partial^2 \psi}{\partial x^2} + \frac{\partial^2 \psi}{\partial y^2} = -Ra\frac{\partial \theta}{\partial x} + RaNr\frac{\partial \varphi}{\partial x}, \tag{17}$$

$$\frac{\partial \psi}{\partial y}\frac{\partial \theta}{\partial x} - \frac{\partial \psi}{\partial x}\frac{\partial \theta}{\partial y} = \left(1 + \frac{4}{3}N_R\right)\left(\frac{\partial^2 \theta}{\partial x^2} + \frac{\partial^2 \theta}{\partial y^2}\right) + Nb\left(\frac{\partial \varphi}{\partial x}\frac{\partial \theta}{\partial x} + \frac{\partial \varphi}{\partial y}\frac{\partial \theta}{\partial y}\right)$$
$$+ Nt\left[\left(\frac{\partial \theta}{\partial x}\right)^2 + \left(\frac{\partial \theta}{\partial y}\right)^2\right] + Ec\left(\left(\frac{\partial \psi}{\partial x}\right)^2 + \left(\frac{\partial \psi}{\partial y}\right)^2\right). \tag{18}$$

$$\frac{\partial \psi}{\partial y}\frac{\partial \varphi}{\partial x} - \frac{\partial \psi}{\partial x}\frac{\partial \varphi}{\partial y} = \frac{1}{Le}\left(\frac{\partial^2 \varphi}{\partial x^2} + \frac{\partial^2 \varphi}{\partial y^2}\right) + \frac{1}{Le}\frac{Nt}{Nb}\left(\frac{\partial^2 \theta}{\partial x^2} + \frac{\partial^2 \theta}{\partial y^2}\right). \tag{19}$$

The corresponding boundary conditions of these equations are given by

$$\psi = 0, \quad \theta = 1, \quad \tilde{J}_p = 0\left(or\ Nb\frac{\partial \varphi}{\partial x} + Nt\frac{\partial \theta}{\partial x} = 0\right) \quad at \quad x = -0.5$$

$$\psi = 0, \quad \theta = 0, \quad \tilde{J}_p = 0\left(or\ Nb\frac{\partial \varphi}{\partial x} + Nt\frac{\partial \theta}{\partial x} = 0\right) \quad at \quad x = 0.5$$

$$\psi = 0, \quad \frac{\partial \theta}{\partial y} = 0, \quad \frac{\partial \varphi}{\partial y} = 0 \quad on \quad y = 0 \quad and \quad y = 1 \tag{20}$$

Here, Ra is the Rayleigh number for the porous medium, Le is the Lewis number, N_R is the radiation parameter, Ec is the Eckert number for the porous medium, Nr is the buoyancy ratio parameter, Nb is the Brownian motion parameter and Nt is thermophoresis parameter, which are defined as

$$Ra = \frac{(1-C_0)gK\rho_{f0}\beta\Delta TL}{\mu\alpha_m}, \quad Le = \frac{\alpha_m}{\varepsilon D_B}, \quad N_R = \frac{4\sigma_{SB}T_\infty^3}{a_R\alpha_m},$$
$$Ec = \frac{\mu\alpha_m}{K(\rho c_p)_f \Delta T}, \quad Nr = \frac{(\rho_p - \rho_{f0})C_0}{\rho_{f0}\beta\Delta T(1-C_0)}, \quad Nb = \frac{\delta D_B C_0}{\alpha_m}, \tag{21}$$
$$Nt = \frac{\delta D_T \Delta T}{\alpha_m T_c}$$

The physical quantities of interest are the local Nusselt number Nu and the local Sherwood number Sh, which are defined as

$$Nu_l = -\left(1 + \frac{4}{3}N_R\right)\left(\frac{\partial \theta}{\partial x}\right)_{x=-0.5}, \quad Sh_l = -\left(\frac{\partial \varphi}{\partial x}\right)_{x=-0.5}$$

$$Nu_r = \left(1 + \frac{4}{3}N_R\right)\left(\frac{\partial \theta}{\partial x}\right)_{x=0.5}, \quad Sh_r = \left(\frac{\partial \varphi}{\partial x}\right)_{x=0.5} \tag{22}$$

Also, the average Nusselt and Sherwood numbers $\bar{N}u$ and $\bar{S}h$ are defined as

$$\bar{N}u_l = \int_0^1 Nu_l dy, \quad \bar{S}h_l = \int_0^1 Sh_l dy, \quad \bar{N}u_r = \int_0^1 Nu_r dy, \quad \bar{S}h_r = \int_0^1 Sh_r dy. \tag{23}$$

It should be noted that the Sherwood number is correlated to the Nusselt number by the boundary conditions through the following relations,

$$Sh_l = \frac{Nt}{\left(1 + \frac{4}{3}N_R\right)Nb}Nu_l \quad and \quad Sh_r = \frac{Nt}{\left(1 + \frac{4}{3}N_R\right)Nb}Nu_r \tag{24}$$

where the above equations are concluded from the employed boundary conditions. Considering Eq. (24) for Sherwood number, the results will be reported for the Nusselt number.

Here, relations of skin friction coefficient is defined as following [28]:

$$\tau_w = \mu_0 \frac{\partial v}{\partial \bar{x}}\bigg|_{\bar{x}=-\frac{L}{2}} \tag{25}$$

where, the nondimensional form of skin friction coefficient for left hot wall is given by:

$$C_{f,l} = \frac{\partial^2 \psi}{\partial x^2}\bigg|_{x=-0.5} \tag{26}$$

3. Numerical method

The system of partial differential equations (PEDs), Eqs. (17)–(19), and the corresponding boundary conditions, Eq. (20), are transformed into the weak form to be solved numerically by the aid of Galerkin finite element method [36]. Employing the basis set, the nondimensional stream function (ψ) variable, nondimensional temperature variable (θ) and the nondimensional concentration (φ) of nanoparticles are expanded as,

$$\psi \approx \sum_{k=1}^{N} \psi_k \omega_k(x, y), \quad \theta \approx \sum_{k=1}^{N} \theta_k \omega_k(x, y), \quad \varphi \approx \sum_{k=1}^{N} \varphi_k \omega_k(x, y), \tag{27}$$

where $-0.5 < x < 0.5$ and $0 < y < 1$.

For all of the three variables the basis function (ω) is the same, and thus, the total number of nodes is N. Then, the nonlinear residual equations are obtained as follow by applying the Galerkin finite element method on the governing equations at the nodes of the internal domain Ω,

$$R_i^1 = \sum_{k=1}^{N} \psi_k \int_{\Omega} \left[\frac{\partial \omega_i}{\partial x} \frac{\partial \omega_k}{\partial x} + \frac{\partial \omega_i}{\partial y} \frac{\partial \omega_k}{\partial y} \right] dxdy - Ra \left(\sum_{k=1}^{N} \theta_k \int_{\Omega} \frac{\partial \omega_k}{\partial x} \omega_i dxdy \right)$$
$$+ RaNr \left(\sum_{k=1}^{N} \varphi_k \int_{\Omega} \frac{\partial \omega_k}{\partial x} \omega_i dxdy \right) \tag{28}$$

$$R_i^2 = \left(\sum_{k=1}^{N} \psi_k \int_{\Omega} \frac{\partial \omega_k}{\partial y} \omega_i dxdy \right) \left(\sum_{k=1}^{N} \theta_k \int_{\Omega} \frac{\partial \omega_k}{\partial x} \omega_i dxdy \right)$$
$$- \left(\sum_{k=1}^{N} \psi_k \int_{\Omega} \frac{\partial \omega_k}{\partial x} \omega_i dxdy \right) \left(\sum_{k=1}^{N} \theta_k \int_{\Omega} \frac{\partial \omega_k}{\partial y} \omega_i dxdy \right)$$
$$+ \left(1 + \frac{4}{3} N_R \right) \sum_{k=1}^{N} \theta_k \int_{\Omega} \left(\frac{\partial \omega_i}{\partial x} \frac{\partial \omega_k}{\partial x} + \frac{\partial \omega_i}{\partial y} \frac{\partial \omega_k}{\partial y} \right)$$
$$+ Nb \left(\sum_{k=1}^{N} \varphi_k \int_{\Omega} \frac{\partial \omega_k}{\partial x} \omega_i dxdy \right) \left(\sum_{k=1}^{N} \theta_k \int_{\Omega} \frac{\partial \omega_k}{\partial x} \omega_i dxdy \right) \tag{29}$$
$$+ Nb \left(\sum_{k=1}^{N} \varphi_k \int_{\Omega} \frac{\partial \omega_k}{\partial y} \omega_i dxdy \right) \left(\sum_{k=1}^{N} \theta_k \int_{\Omega} \frac{\partial \omega_k}{\partial y} \omega_i dxdy \right)$$
$$+ Nt \left[\left(\sum_{k=1}^{N} \theta_k \int_{\Omega} \frac{\partial \omega_k}{\partial x} \omega_i dxdy \right)^2 + \left(\sum_{k=1}^{N} \theta_k \int_{\Omega} \frac{\partial \omega_k}{\partial y} \omega_i dxdy \right)^2 \right]$$
$$+ Ec \left[\left(\sum_{k=1}^{N} \psi_k \int_{\Omega} \frac{\partial \omega_k}{\partial x} \omega_i dxdy \right)^2 + \left(\sum_{k=1}^{N} \psi_k \int_{\Omega} \frac{\partial \omega_k}{\partial y} \omega_i dxdy \right)^2 \right]$$

and

$$R_i^3 = Le \left(\sum_{k=1}^{N} \psi_k \int_{\Omega} \frac{\partial \omega_k}{\partial y} \omega_i dxdy \right) \left(\sum_{k=1}^{N} \varphi_k \int_{\Omega} \frac{\partial \omega_k}{\partial x} \omega_i dxdy \right)$$
$$- Le \left(\sum_{k=1}^{N} \psi_k \int_{\Omega} \frac{\partial \omega_k}{\partial x} \omega_i dxdy \right) \left(\sum_{k=1}^{N} \varphi_k \int_{\Omega} \frac{\partial \omega_k}{\partial y} \omega_i dxdy \right)$$
$$+ \sum_{k=1}^{N} \varphi_k \int_{\Omega} \left(\frac{\partial \omega_i}{\partial x} \frac{\partial \omega_k}{\partial x} + \frac{\partial \omega_i}{\partial y} \frac{\partial \omega_k}{\partial y} \right) \tag{30}$$
$$+ \frac{Nt}{Nb} \sum_{k=1}^{N} \theta_k \int_{\Omega} \left(\frac{\partial \omega_i}{\partial x} \frac{\partial \omega_k}{\partial x} + \frac{\partial \omega_i}{\partial y} \frac{\partial \omega_k}{\partial y} \right)$$

where R_i are the nonlinear residual equations. Here, the Bi-quadratic functions with three point Gaussian quadrature is employed for evaluating the integrals. The Newton–Raphson method is also applied to solve the nonlinear residual equations, R_i, for the coefficients of the expansions, i.e. ψ_k, θ_k and φ_k, in Eq. (27). More details about the solution procedure can be found in the excellent studies by Reddy [36] and Basak et al. [37,38]. In the present study, a nonuniform grid, in which the grid points are symmetrically clustered next to the vertical and horizontal walls with the ratio of 1.05, is utilized. The zero

Table 1
Comparison of the average Nusselt number of the hot wall.

References	Ra		
	10	100	1000
[39]	–	3.097	12.96
[40]	1.079	3.16	14.06
[41]	–	3.113	–
[42]	–	3.141	13.448
[43]	–	4.2	15.8
[44]	–	3.118	13.637
[45]	1.065	2.801	–
Present results	1.08	3.11	13.64

values for the stream function, the value of 1/2 for the temperature, and unity for the concentration is adopted as initial guesses. Starting from the initial guesses, the system of residual equations were solved iteratively and the calculations were repeated until the residuals for the field variables, i.e. stream function, temperature and concentrations, become small (10^{-7} or lower). The solution procedure, in the form of an in-house computational fluid dynamics (CFD) code, has been validated successfully against the results available in literature.

3.1. Code validation

Neglecting the effect of nanoparticles, the present study is limited to the study of pure fluid in a square enclosure. In this case, the numerical results are compared with the previous studies in Table 1. As seen, the results are in good agreement with the results available in literature.

3.2. Grid check

In the present study, the results were reported for Rayleigh number in the range of $10 < Ra < 1000$, the buoyancy ratio in the range of $0 < Nr < 90$, the radiation parameter N_R in the range of $0 < N_R < 1$, the Eckert number in the range of $0 < E_c < 0.01$ [46]. The value of thermophoresis and Brownian parameters are discussed in [47] and found that they are small about 10^{-6}. The Lewis number is large of the order 1000 and higher [47]. Here, the results were computed for various combinations of the nondimensional parameters and various mesh sizes. The summery of the calculations for various values of Ec, N_R, Le is shown in Table 2 when $Nr = 20$, $Nb = Nt = 10^{-6}$, $Ra = 1000$. According to the results of Table 2, the grid size of 125×125 could provide sufficient accuracy for results. Hence, this size of grid is employed for calculations.

4. Results and discussion

In the following text, the results are reported for a typical case of $Ra = 100$, $Ec = 0.001$, $\varepsilon = 0.7$, $N_R = 1/4$, $Nb = $ 1E-6, $Nt = $ 1E-6, $Le = 1000$ and $Nr = 20$, otherwise the value of nondimensional parameter will be stated.

Figs. 2, 3 and 4 show the effect of viscous dissipation on the streamlines, isotherms and iso-concentrations for two Eckert numbers of $Ec = 0$ and $Ec = 0.001$. Fig. 2 clearly shows the circulation of the nanofluid in the cavity. As seen in this figure, the presence of viscous dissipation effects tends to shift the streamlines toward the core. The most significant effect of the presence of viscous dissipation effects (i.e. $Ec = 0.001$) can be seen about the top-left corner as well as the bottom-right corner, where the velocities of flow are high. Fig. 3 indicates that the presence of viscous dissipation effects tend to increase the temperature in the vicinity of the hot wall. This figure in agreement with Fig. 2 shows that the most significant effect

Table 2
Grid independency for different combination of nondimensional parameters.

			Average Nusselt number (hot walls $\bar{Nu}_l$)					
			Grid size					
Ec	N_R	Le	50×50	75×75	100×100	125×125	150×150	200×200
0	0	100	2.6833	2.683	2.6828	2.6828	2.6828	2.6827
0.001	0.5	100	3.3182	3.3177	3.3176	3.3175	3.3175	3.3174
0.001	0.5	1000	3.5479	3.5474	3.5472	3.5471	3.5471	3.547
0.005	0.5	1000	2.9095	2.9110	2.9114	2.9114	2.9114	2.9113

is about the top-left and bottom right corners where the temperature profiles are under the significant effect of viscous dissipation. Fig. 4 compares the nondimensional distribution of nanoparticles in the cavity when the viscous dissipation effects are negligible (see Fig. 4a) and when they are significant (see Fig. 4b). Fig. 4a shows a significant gradient of nanoparticles next to hot and cold walls. As seen in Fig. 3, the temperature gradient next to the hot and cold vertical walls is high, and hence, the thermophoresis force is high in the vicinity of the vertical walls. Thus, next to the hot wall, the thermophoresis force tends to move the nanoparticles away from the wall. In contrast, the thermophoresis force near the cold wall tends to push the nanoparticles into the cold wall. Hence, the concentration of nanoparticles near the hot wall is low and near the cold wall is high. The concentration of nanoparticles near the top wall is also low. This is mostly because of the flow in the cavity. The flow near the low concentration hot wall is toward the top wall. Indeed, when the flow is near the hot wall, the nanoparticles are subject to the thermophoresis force and tend to move in the opposite direction of the temperatures gradients. As the flow of nanofluid continues to flow toward the top wall, more and more nanoparticles get away from the wall until the low concentration nanofluid reaches the top wall. As a result, the flow with low concentration of nanoparticles will be collected near the top wall. The opposite behavior could be seen near the cold wall. For the cold wall, it should be noticed that the nanoparticles tend to be collected near the wall due to the thermophoresis force, and hence, the cold bottom wall contains high concentration of nanoparticles. Comparison between Fig. 4a and 4b reveals that the presence of viscous dissipation effects tends to uniform the concentration in the cavity and reduce the concentration gradients.

Figs. 5, 6 and 7 illustrate the effect of radiation parameter (N_R) on the streamlines, isotherms and iso-concentrations. Fig. 5 shows that the presence of radiation effects mostly affects the streamlines in the core region of the cavity where the flow is weak. Fig. 6 shows the radiation effects on the temperature profiles. The presence of radiation effects induces significant influences on the temperature profiles next to the horizontal walls. This is the place, in which there is a significant temperature difference in vertical direction and the flow velocity is low. Attention to the temperature distribution for $N_R = 0$ and $N_R = \frac{1}{4}$ next to the vertical walls shows that the dashed green lines are smoothly closer to the vertical walls compared to the solid red ones, which means that the temperature gradient in the absence of radiation effects is smoothly higher in the mentioned places. Indeed, the presence of radiation effects increases the effective thermal conductivity of the porous medium and the nanofluid. When the thermal conductivity increases, the heat could easily transfer better from the vertical walls into the cavity and the temperature difference reduces. It is worth noticing that although the presence of radiation effects tends to reduce the temperature gradients, the increase of the effective thermal conductivity tends to increase the Nusselt number (see Eq. (24)).

Fig. 7 shows the distribution of nanoparticles in the cavity when the radiation effects are negligible ($N_R = 0$ and $Ec = 0.001$). The results of this figure could be compared with the results of Fig. 4a (i.e. $Ec = 0.001$ and $N_R = \frac{1}{4}$). The comparison between these two figures indicates that the influence of the radiation effect on the distribution of nanoparticles is very smooth.

Fig. 8 shows the local values of Nusselt number at (a): the hot wall and (b): the cold wall for different values of Eckert number and radiation parameter. As seen, the Nusselt number at the bottom of
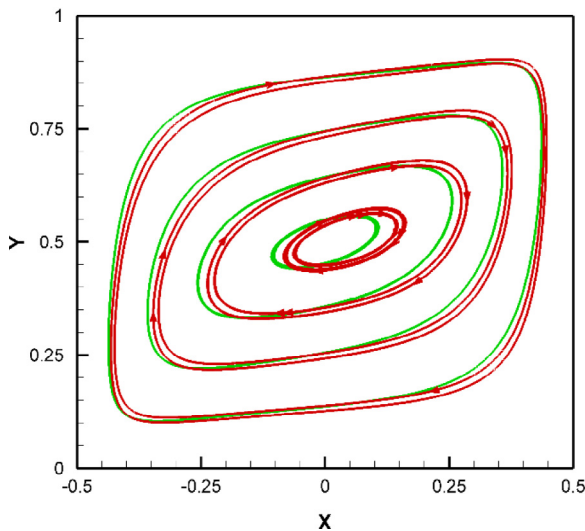
Fig. 2. The streamlines for two values of Eckert number: $Ec = 0$ (the green lines) and $Ec = 0.005$ (the red lines with arrows).
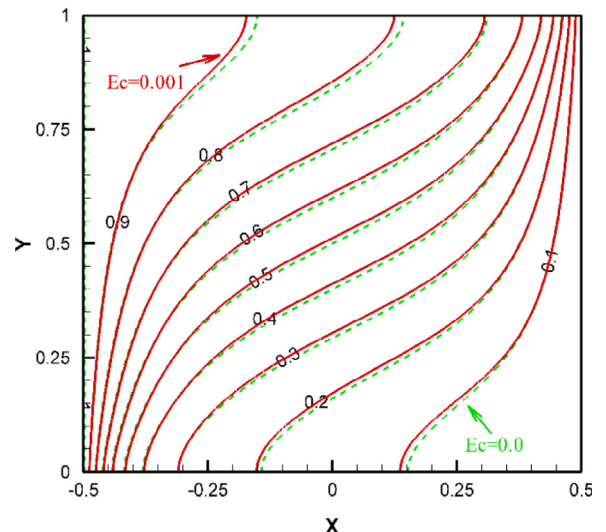
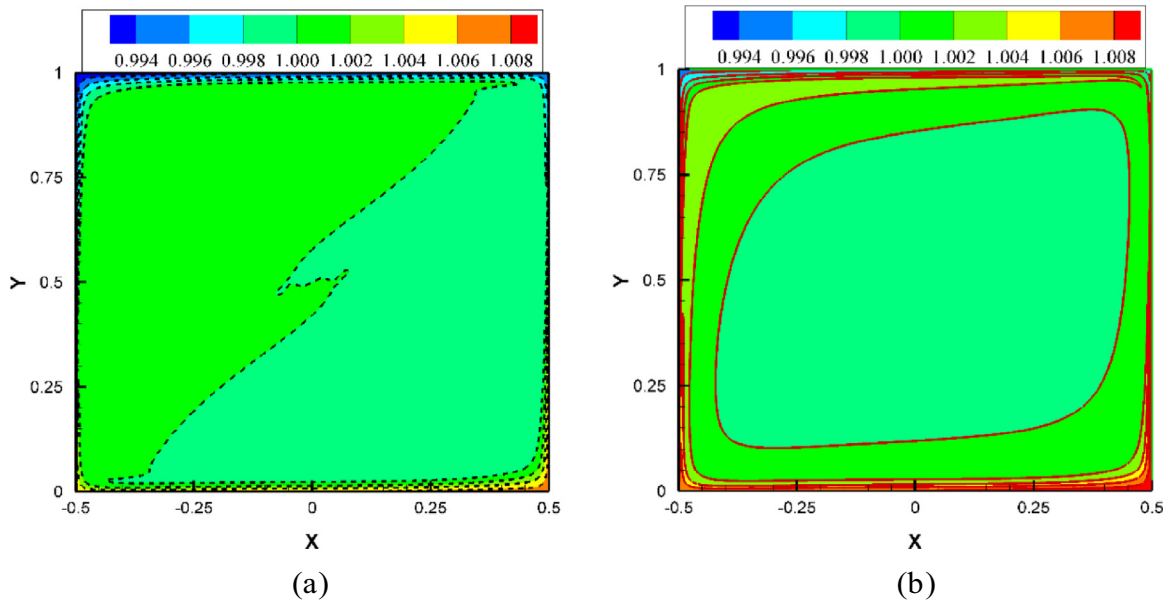**Fig. 3.** The isotherms for two values of Eckert number: $Ec = 0$ and $Ec = 0.005$.

Fig. 4. The concentration for two values of Eckert number: (a) $Ec = 0$ and (b) $Ec = 0.001$.

the hot wall (i.e. $y \approx 0$) is very high; this is where the high concentration of fresh cold nanofluid commenced to flow over the wall. As the nanofluid moves toward the top, the Nusselt number starts to reduce. Hence, the minimum value of the local Nusselt number can be seen next to the top wall (i.e. $y \approx 1$). The similar trend of behavior can be seen for the cold wall but in the reverse direction. For the sake of better comparison, the results for the cold wall are plotted as a function of $(1-y)$ in Fig. 8b. For the hot wall, Fig. 8a indicates that the increase of the radiation parameter (N_R) decreases the local Nusselt number (comparison between the dash-dot blue line and dash-dot-dot orange line). Similar trend of behavior could also be seen for the Eckert number (comparison between the dash green line and dash-dot blue line). It is also clear that the maximum value of the Nusselt number next to the bottom wall (i.e. $y \approx 0$) decreases when the viscous effects (e.g. $Ec = 0.001$) and the radiation effects ($N_R = 1.0$) are significant. It is also interesting that the presence of the viscous dissipation and radiation effects tend to increase the local Nusselt number near the top wall. This is because of the fact that the presence of viscous and radiation effects would increase the overall temperature of the nanofluid in the vicinity of the wall, which consequently, results in higher buoyancy forces, and ultimately, the stronger the buoyancy flow the stronger the surface heat transfer (higher local Nusselt number). Fig. 8b illustrates that the magnitude of the local Nusselt number at the top of the cold wall (i.e. $(1-y) \approx 0$) is higher than that of the bottom of the hot wall (i.e. $y \approx 0$) when $N_R = 1.0$ and $Ec = 0.0$. Indeed, the presence of viscous dissipation generates significant amount of heat in the cavity, which should be extracted from the cold wall. It is clear that when the viscous dissipation is negligible (i.e. $Ec = 0$), the local Nusselt number for the hot and cold walls are the same.

Fig. 9 shows the influence of the radiation parameter on the average Nusselt number at the hot and cold walls for various values of Eckert number. This figure shows that the increase of the viscous dissipation (i.e. Eckert number) decreases the average Nusselt
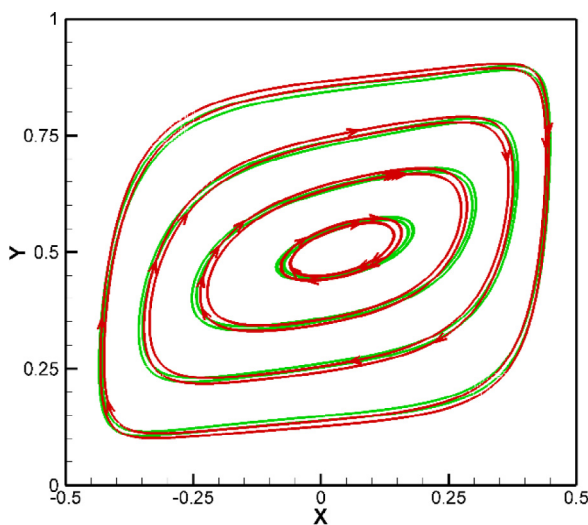

Fig. 5. The streamlines for two values of N_R parameter: $N_R = 0$ (the green lines) and $N_R = {}^1/_4$ (the red lines with arrows).
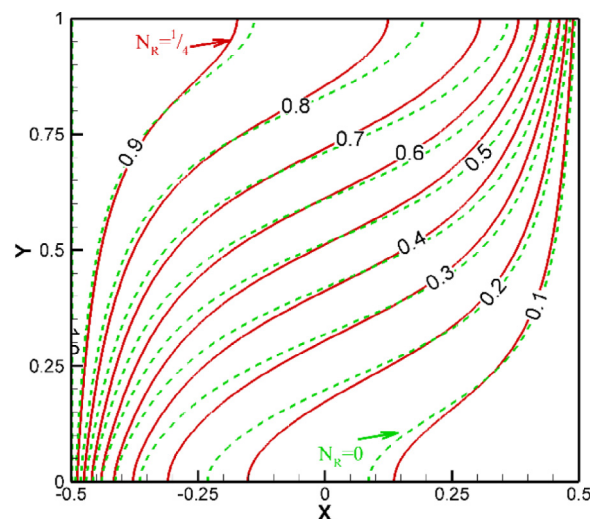

Fig. 6. The isotherms for two values of N_R parameter: $N_R = 0$ and $N_R = {}^1/_4$.
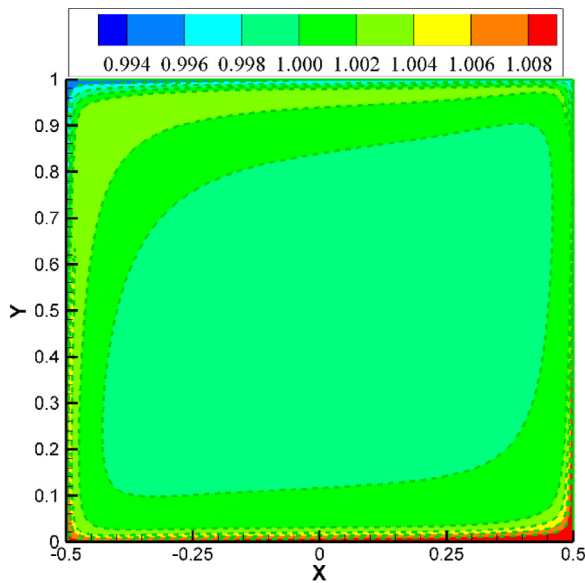
Fig. 7. The concentration distribution when $N_R = 0$.

Fig. 9. Average Nusselt number at hot wall as a function of radiation parameter (N_R) for various values of Eckert number (Ec).

number at the hot wall. In contrast, the average Nusselt number at the cold wall is an increasing function of viscous dissipation (Ec). Indeed, the viscous dissipation tends to increase the temperature of the fluid next to hot wall, which consequently, reduces the temperature difference between the hot wall and the adjacent fluid. As a result, the presence of viscous dissipation tends to reduce the average Nusselt number for the hot wall. The viscous dissipation would also increase the temperature of the fluid next to the cold wall, which results in the increase of temperature difference and the increase of Nusselt number at the cold side.

Fig. 10 shows the average Nusselt number as a function of buoyancy ratio parameter (Nr) for different values of radiation parameter (N_R). This figure in agreement with Fig. 9 shows that the presence of radiation effects increases the average Nusselt number. Attention to isotherms in Figs. 3 and 6 shows that the presence of radiation effects tend to reduce the gradient of temperature at the wall; however, the presence of radiation effects also tend to increase the
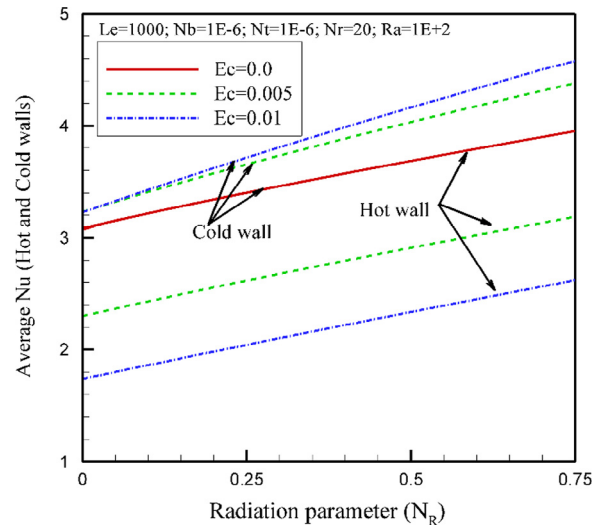
heat transfer by the increase of the effective thermal diffusion in the porous medium. This figure shows that the increase of the heat diffusion due to radiation is the dominant effect, and hence, the average Nusselt numbers is an increasing function of radiation parameter (N_R). This figure also reveals that the raise of the buoyancy ratio parameter reduces the average Nusselt number.

Fig. 11 shows the effect of Lewis and Eckert numbers on the average Nusselt number at the hot wall. This figure indicates that the increase of Lewis number increases the heat transfer from the wall (i.e. average Nu). When the Lewis number is small about 100 or lower, the increase of average Nusselt by the increase of Lewis number is significant, but the increase of Lewis number to values above 100 shows only smooth enhancement in the heat transfer from the surface (i.e. average Nu). When the Lewis number is small, the thickness of the boundary layer for concentration of nanoparticles over the vertical walls is large, and hence, a large area of the cavity is under the influence of the migration of nanofluids. When the Lewis number increases, the thickness of the concentration boundary layer
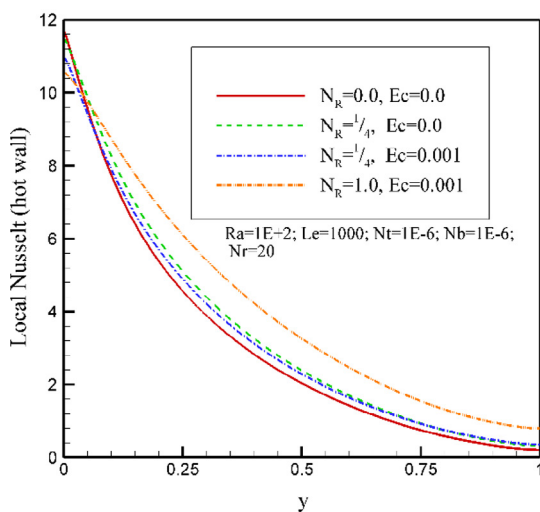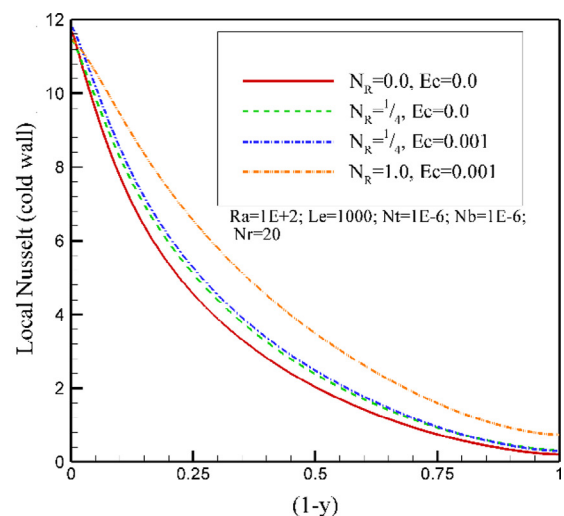
Fig. 8. Local Nusselt number at the hot and cold walls for different values of Eckert number and radiation parameter: (a) hot wall and (b) cold wall.
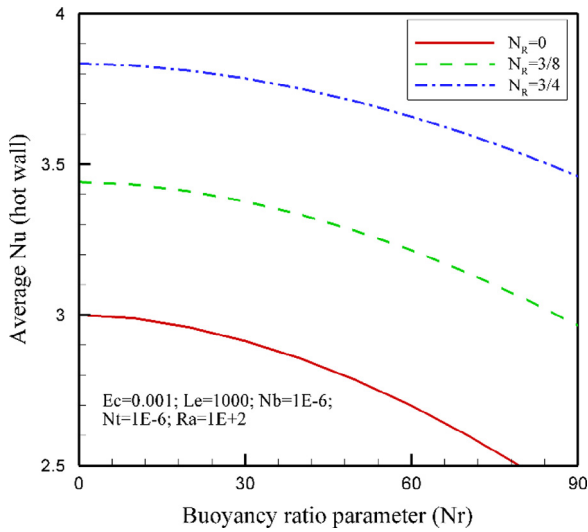
Fig. 10. Average Nusselt number at hot wall as a function of buoyancy ratio parameter (Nr) for various values of radiation parameter (N_R).

Fig. 12. A comparison between contour of isotherms of $Nt = 3\text{E-}6$, $Nb = 1\text{E-}6$ (red dashed line) and $Nt = 1\text{E6}$, $Nb = 3\text{E-}6$ (green continues line) when $Ra = 100$, $Ec = 0.001$, $\varepsilon = 0.7$, $N_R = 1/4$, $Le = 1000$, $Nr = 20$.

over the vertical walls decreases, and consequently, the affective area of migration of nanoparticles also decreases. For very large values of Lewis number, the concentration boundary layer is a very narrow region next to the vertical walls, and hence, further increase of Lewis number does not show significant effect on the heat transfer from the wall (i.e. average Nusselt number).

Here, three sets of Nt and Nb parameters have been defined as: I: $Nt = Nb = 1\text{E-}6$, II: $Nt = 1\text{E-}6$, $Nb = 3\text{E-}6$ and III: $Nt = 3\text{E-}6$, $Nb = 1\text{E-}6$. Figs. 12, 13 and 14 depict the isotherm contours, the iso-concentration contours and the streamlines for the sets of II (i.e. $Nt = 1\text{E-}6$, $Nb = 3\text{E-}6$) and III (i.e. $Nt = 3\text{E-}6$, $Nb = 1\text{E-}6$). As seen, the variation of Nt and Nb induces a significant effect on the isotherms, concentration contours and the streamlines. As seen, as the Thermophoresis effect gets stronger (e.g. the case of $Nt = 3\text{E-}6$, $Nb = 1\text{E-}6$), the concentration distribution of nanoparticles in the cavity gets more nonuniform. Fig. 15 shows the effect of Thermophoresis and Brownian parameters on the local Nusselt number (Fig. 15a) and skin friction (Fig. 15b) at the left hot wall. In these figures, the results are plotted for those three mentioned
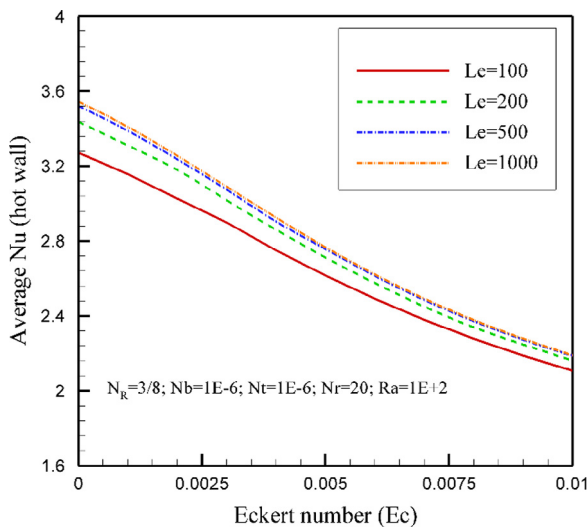
sets of Nt and Nb parameters. Fig. 15a indicates that the effect of fluctuation of Nt on the local Nusselt number is more significant at the bottom of hot wall than the top of the wall. Indeed, the themophoresis force drives nanoparticles from hot wall toward the cold wall. Near the bottom of the hot wall is the area where the fresh stream of the cold flow reaches the hot surface, and hence, the temperature gradient is high. The increase of the temperature gradient boosts the thermophoresis effect and induces a significant effect on the local Nusselt number. As the cold fluid flows toward the top, it gets hot and the temperature gradient drops. Near the top of the wall, the temperature gradient is low, and consequently, the thermophoresis effect is also weak. Thus, as seen in Fig. 15a, there is a significant effect on the local Nusselt number at the bottom of the wall (i.e. length of hot wall near zero), and by moving toward the top of the wall the impact of thermophoresis parameter on the local Nusselt number decreases. It is also clear that the fluctuation of Brownian motion parameter induces a negligible effect on the variation of the local Nusselt number.

Fig. 15b shows the profiles of the skin friction at the hot wall. As seen, the increase of the thermophoresis parameter or the decrease of the Brownian motion parameter results in increase of the wall skin friction. Indeed, the increase of the thermophoresis parameter boosts the effect of temperature gradient and increases the migration of nanoparticles from the vicinity of the hot wall into the colder areas. As the heavy nanoparticles move away from the wall, the fluid near the hot wall gets lighter and the buoyancy forces get stronger. Thus, by the increase of the thermophoresis force, the skin friction increases. In contrast, the increase of the Brownian motion parameter tends to uniform the nanoparticles near the wall and reduces the buoyancy effect. Hence, as seen, the increase of the Brownian motion parameter reduces the skin friction.

5. Conclusion

The radiation and viscous dissipation effects on the convective heat transfer of nanofluids in a cavity is studied using Buongiorno's mathematical model for nanofluids. The Darcy–Boussinesq model is utilized for modeling the flow in the porous media. The governing equations are transformed into a nondimensional form and successfully solved using the finite element method. The local and average Nusselt number at the hot and cold walls were calculated and reported for various values of the radiation parameter (N_R) as

Fig. 11. Average Nusselt number at hot wall as a function of Eckert number (Ec) for various values of Lewis number.

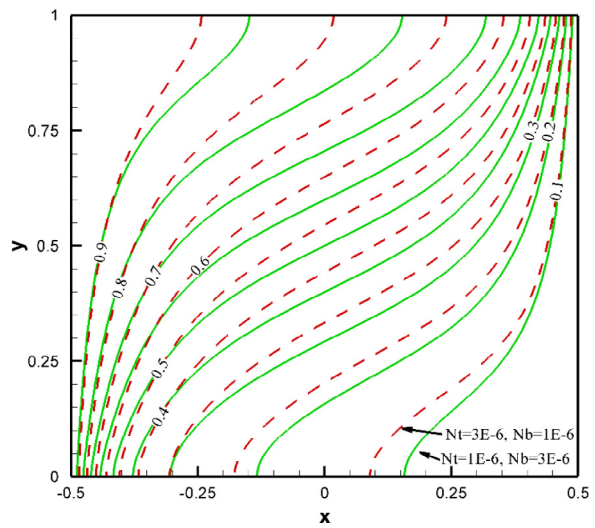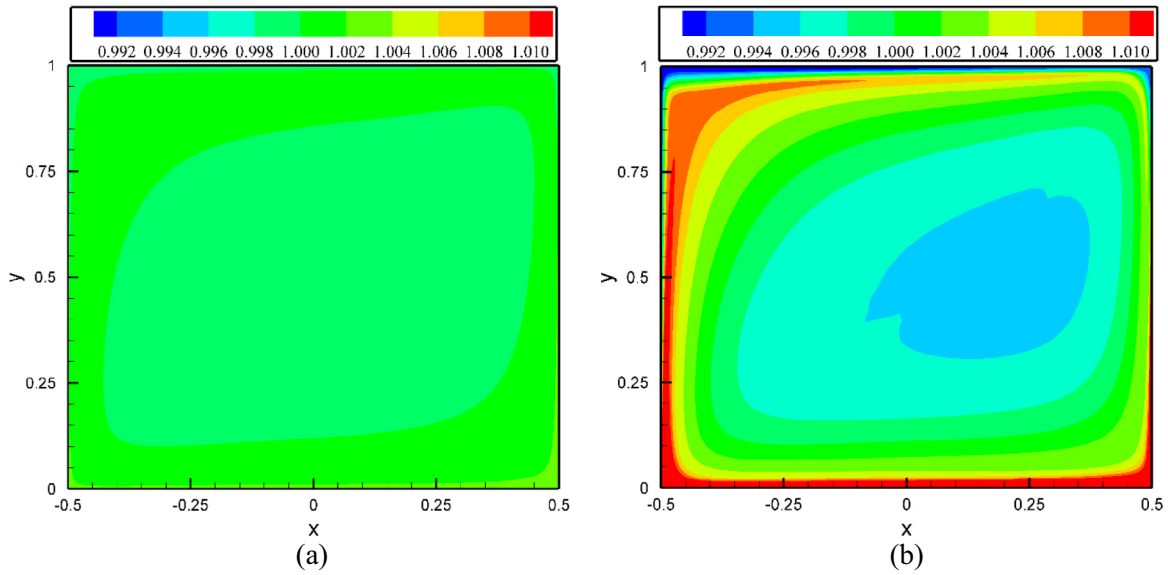**Fig. 13.** A comparison between nanoparticles concentration profiles: (a) $Nt = 1E\text{-}6$, $Nb = 3E\text{-}6$ and (b) $Nt = 3E\text{-}6$, $Nb = 1E\text{-}6$ when $Ra = 100$, $Ec = 0.001$, $\varepsilon = 0.7$, $N_R = 1/4$, $Le = 1000$, $Nr = 20$.

well as viscous dissipation effect (Ec). The main outcomes of the present study could be summarized as:

1. The effect of viscous dissipation on the concentration distribution of nanoparticles is significant.
2. The presence of viscous dissipation results in higher values of average Nusselt number at the cold wall. The raise of viscous dissipation (Ec) tends to reduce the average Nusselt number at the hot wall.
3. The presence of radiation effect reduces the temperature gradient but increases the heat diffusion in the porous media and nanofluid. It is found that the overall effect of the presence of radiation effect is to increase the heat transfer (average Nusselt number).
4. The increase of Lewis number and buoyancy ratio parameter, respectively, increases and decreases the average Nusselt number.
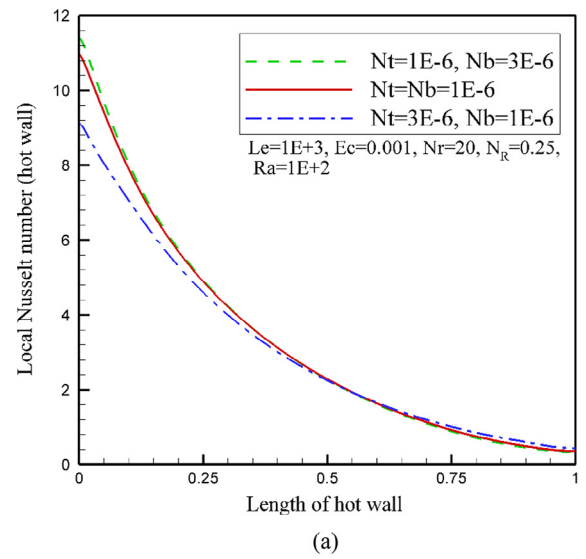
(a)
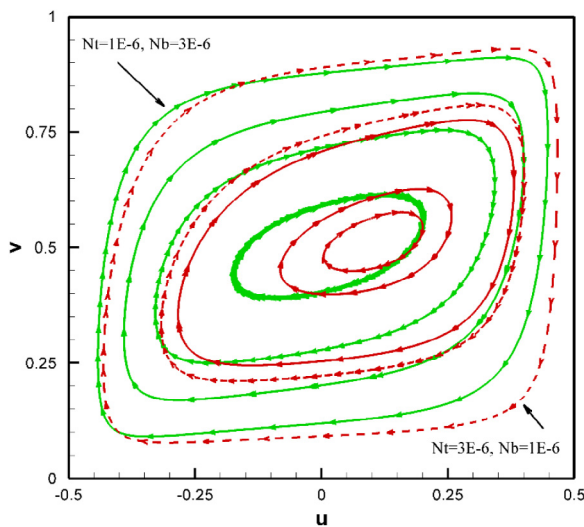
Fig. 14. A comparison between stream functions of $Nt = 3E\text{-}6$, $Nb = 1E\text{-}6$ (red dashed lines) and $Nt = 1E\text{-}6$, $Nb = 3E\text{-}6$ (green continues lines) when $Ra = 100$, $Ec = 0.001$, $\varepsilon = 0.7$, $N_R = 1/4$, $Le = 1000$, $Nr = 20$.
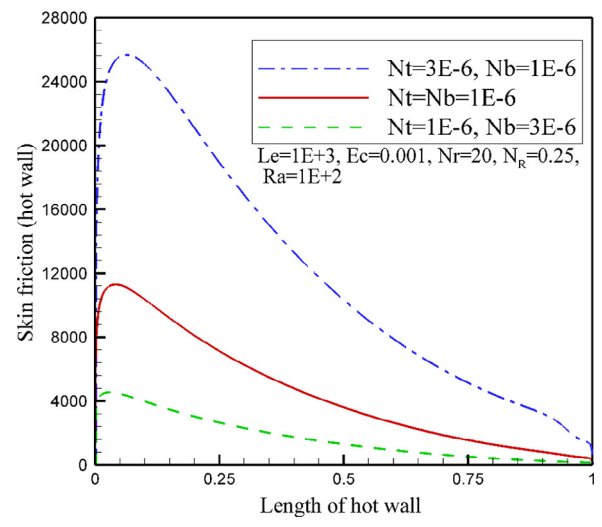
(b)

Fig. 15. Effects of Thermophoresis and Brownian parameters on the vertical hot wall: (a) local Nusselt number and (b) local skin friction.

5. Augmentation of thermophoresis parameter results in a low value of heat transfer (Nusselt number) and high value of skin friction (gradient of velocity of nanofluid).

Acknowledgements

References

[1] K. Vafai (Ed.), Handbook of Porous Media, CRC Press, Boca Raton, FL, 2005.
[2] W. Lu, C.Y. Zhao, S.A. Tassou, Thermal analysis on metal-foam filled heat exchangers. Part I: metal-foam filled pipes, Int. J. Heat Mass Transf. 49 (15) (2006) 2751–2761.
[3] A. Bhattacharya, R.L. Mahajan, Metal foam and finned metal foam heat sinks for electronics cooling in buoyancy-induced convection, J. Electron. Packag. 128 (3) (2006) 259–266.
[4] Z. Luo, C. Wang, W. Wei, G. Xiao, M. Ni, Performance improvement of a nanofluid solar collector based on direct absorption collection (DAC) concepts, Int. J. Heat Mass Transf. 75 (2014) 262–271.
[5] M. Karami, M.A. Akhavan-Bahabadi, S. Delfani, M. Raisee, Experimental investigation of CuO nanofluid-based direct absorption solar collector for residential applications, Renew. Sustain. Energy Rev. 52 (2015) 793–801.
[6] A. Menbari, A.A. Alemrajabi, Analytical modeling and experimental investigation on optical properties of new class of nanofluids (Al_2O_3–CuO binary nanofluids) for direct absorption solar thermal energy, Opt. Mater. 52 (2016) 116–125.
[7] Q. Sun, I. Pop, Free convection in a triangle cavity filled with a porous medium saturated with nanofluids with flush mounted heater on the wall, Int. J. Therm. Sci. 50 (2011) 2141–2153.
[8] M. Ghalambaz, M.A. Sheremet, I. Pop, Free convection in a parallelogrammic porous cavity filled with a nanofluid using Tiwari and Das' nanofluid model, PLoS ONE 10 (2015) e0126486.
[9] A. Noghrehabadi, A. Behseresht, M. Ghalambaz, J. Behseresht, Natural-convection flow of nanofluids over vertical cone embedded in non-Darcy porous media, J. Thermophys. Heat Transfer 27 (2013) 334–341.
[10] A. Noghrehabadi, A. Behseresht, M. Ghalambaz, Natural convection of nanofluid over vertical plate embedded in porous medium: prescribed surface heat flux, Appl. Math. Mech. 34 (2013) 669–686.
[11] A. Noghrehabadi, M. Ghalambaz, A. Ghanbarzadeh, Effects of variable viscosity and thermal conductivity on natural-convection of nanofluids past a vertical plate in porous media, J. Mech. 30 (2014) 265–275.
[12] M. Ghalambaz, A. Noghrehabadi, Effects of heat generation/absorption on natural convection of nanofluids over the vertical plate embedded in a porous medium using drift-flux model, J. Comput. Appl. Res. Mech. Eng. 3 (2014) 113–123.
[13] M. Ghalambaz, A. Noghrehabadi, A. Ghanbarzadeh, Natural convection of nanofluids over a convectively heated vertical plate embedded in a porous medium, Braz. J. Chem. Eng. 31 (2014) 413–427.
[14] H. Zargartalebi, A. Noghrehabadi, M. Ghalambaz, I. Pop, Natural convection boundary layer flow over a horizontal plate embedded in a porous medium saturated with a nanofluid: case of variable thermophysical properties, Transp. Porous Media 107 (2015) 153–170.
[15] H. Zargartalebi, M. Ghalambaz, A. Noghrehabadi, A. Chamkha, Stagnation-point heat transfer of nanofluids toward stretching sheets with variable thermophysical properties, Adv. Powder Technol. 26 (2015) 819–829.
[16] M.A. Sheremet, I. Pop, Conjugate natural convection in a porous cavity filled by a nanofluid using Buongiorno's mathematical model, Int. J. Heat Mass Transf. 79 (2014) 137–145.
[17] M.A. Sheremet, T. Grosan, I. Pop, Free convection in a square cavity filled with a porous medium saturated by nanofluid using Tiwari and Das' nanofluid model, Transp. Porous Media 106 (2015) 595–610.
[18] M.A. Sheremet, I. Pop, Natural convection in a square porous cavity with sinusoidal temperature distributions on both side walls filled with a nanofluid: Buongiorno's mathematical model, Transp. Porous Media 105 (2014) 411–429.
[19] N.H. Saeid, I. Pop, Viscous dissipation effects on free convection in a porous cavity, Int. Commun. Heat Mass Transf. 31 (2004) 723–732.
[20] M.A. Hussain, I. Pop, Radiation effect on Darcy free convection flow along an inclined surface placed in porous media, Heat Mass Transf. 32 (1997) 223–227.
[21] A. Mahdy, A.J. Chamkha, Chemical reaction and viscous dissipation effects on Darcy–Forchheimer mixed convection in a fluid saturated porous media, Int. J. Numer. Methods Heat Fluid Flow 20 (2010) 924–940.
[22] C. RamReddy, P.V. Murthy, A.J. Chamkha, A.M. Rashad, Influence of viscous dissipation on convection in a non-Darcy porous medium saturated with nanofluid in the presence of magnetic field, Open Transp. Phenom. J. 5 (2013) 20–29.
[23] A.J. Chamkha, A.M. Rashad, C. RamReddy, P.V. Murthy, Viscous dissipation and magnetic field effects in a non-Darcy porous medium saturated with a nanofluid under convective boundary condition, Spec. Top. Rev. Porous Media 5 (2014) 27–39.
[24] A.M. Rashad, A.J. Chamkha, C. RamReddy, P.V. Murthy, Influence of viscous dissipation on mixed convection in a non-Darcy porous medium saturated with a nanofluid, Heat Transfer Asian Res. 43 (2014) 397–411.
[25] T. Hussain, T. Hayat, S.A. Shehzad, A. Alsaedi, B. Chen, A model of solar radiation and joule heating in flow of third grade nanofluid, Z. Naturforsch. 70 (3) (2015) 177–184.
[26] S.A. Shehzad, Z. Abdullah, A. Alsaedi, F.M. Abbasi, T. Hayat, Thermally radiative three-dimensional flow of Jeffrey nanofluid with internal heat generation and magnetic field, J. Magn. Magn. Mater., 397, 108–114 (2016).
[27] S.A. Shehzad, Z. Abdollah, F.M. Abbasi, T. Hayat, A. Alsaedi, Magnetic field effect in three dimensional flow of an Oldroyd-B nanofluid over a radiative surface, J. Magn. Magn. Mater. 399 (2016) 97–108.
[28] O.D. Makinde, W.A. Khan, J.R. Culham, MHD variable viscosity reacting flow over a convectively heated plate in a porous medium with thermophoresis and radiative heat transfer, Int. J. Heat Mass Transf. 93 (2016) 595–604.
[29] O.D. Makinde, Effects of viscous dissipation and Newtonian heating on boundary layer flow of nanofluids over a flat plate, Int. J. Num. Methods Heat Fluid Flow 23 (8) (2013) 1291–1303.
[30] T.G. Motsumi, O.D. Makinde, Effects of thermal radiation and viscous dissipation on boundary layer flow of nanofluids over a permeable moving flat plate, Phys. Scr. 86 (2012) 045003(8pp).
[31] S. Khamis, O.D. Makinde, Y. Nkansah-Gyekye, Unsteady flow of variable viscosity Cu-water and Al_2O_3-water nanofluids in a porous pipe with buoyancy force, Int. J. Num. Methods Heat Fluid Flow 25 (7) (2015) 1638–1657.
[32] A.V. Kuznetsov, D.A. Nield, The Cheng–Minkowycz problem for natural convective boundary layer flow in a porous medium saturated by a nanofluid: a revised model, Int. J. Heat Mass Transf. 65 (2013) 682–685.
[33] D.A. Nield, A.V. Kuznetsov, Thermal instability in a porous medium layer saturated by a nanofluid: a revised model, Int. J. Heat Mass Transf. 68 (2014) 211–214.
[34] J. Buongiorno Convective transport in nanofluids. ASME J. Heat Transf., 128, 240–250 (2006).
[35] A. Raptis, Radiation and free convection flow through a porous medium, Int. J. Comm. Heat Mass Transfer 25 (1998) 289–295.
[36] J.N. Reddy, An Introduction to the Finite Element Method, McGraw-Hill, New York, 1993.
[37] T. Basak, S. Roy, A.R. Balakrishnan, Effects of thermal boundary conditions on natural convection flows within a square cavity, Int. J. Heat Mass Transf. 49 (2006) 4525–4535.
[38] T. Basak, S. Roy, T. Paul, I. Pop, Natural convection in a square cavity filled with a porous medium: effects of various thermal boundary conditions, Int. J. Heat Mass Transf. 49 (2006) 1430–1441.
[39] K.L. Walker, G.M. Homsy, Convection in a porous cavity, J. Fluid Mech. 87 (1978) 338–363.
[40] A.C. Baytas, I. Pop, Free convection in oblique enclosures filled with a porous medium, Int. J. Heat Mass Transf. 42 (1999) 1047–1057.
[41] C. Beckermann, R. Viskanta, S. Ramadhyani, A numerical study of non-Darcian natural convection in a vertical enclosure filled with a porous medium, Numer. Heat Transfer 10 (1986) 446–469.
[42] R. Gross, M.R. Bear, C.E. Hickox, The application of flux-corrected transport (FCT) to high Rayleigh number natural convection in a porous medium, in: Proc. 7th IHTC, San Francisco, CA, 1986.
[43] A. Bejan, On the boundary layer regime in a vertical enclosure filled with a porous medium, Lett. Heat Mass Transf. 6 (1979) 82–91.
[44] D.M. Manole, J.L. Lage, Numerical benchmark results for natural convection in a porous medium cavity, in: Heat Mass Transfer Porous Media, ASME Conference, vol. 105, 1992, pp. 44–59.
[45] S.L. Moya, E. Ramos, M. Sen, Numerical study of natural convection in a tilted rectangular porous material, Int. J. Heat Mass Transf. 30 (1987) 630–645.
[46] I.A. Badruddin, Z.A. Zainal, Z.A. Khan, Z. Mallick, Effect of viscous dissipation and radiation on natural convection in a porous medium embedded within vertical annulus, Int. J. Therm. Sci. 46 (2007) 221–227.
[47] A. Behseresht, A. Noghrehabadi, M. Ghalambaz, Natural-convection heat and mass transfer from a vertical cone in porous media filled with nanofluids using the practical ranges of nanofluids thermo-physical properties, Chem. Eng. Res. Des. 92 (2014) 447–452.